2023 IEEE Symposium on Electromagnetic Compatibility & Signal/Power Integrity (EMC+SIPI) | 979-8-3503-0976-8/23/$31.00 ©2023 IEEE | DOI: 10.1109/EMCSIPI50001.2023.10241617

dV/dt Impact on Turn-to-Turn Overvoltage Distribution in Motor Windings

Yalda Azadeh
Electrical Engineering
Stony Brook University
Stony Brook, USA
yalda.azadeh@stonybrook.edu

Abdul Basit Mirza
Electrical Engineering
Stony Brook University
Stony Brook, USA
abdulbasit.mirza@stonybrook.edu

Kushan Choksi
Electrical Engineering
Stony Brook University
Stony Brook, USA
choksi.kushan@stonybrook.edu

Xiaolong Zhang
Electrical Engineering
University of Illinoins
Urbana Champaign, USA
xzhng157@illinois.edu

Fang Luo
Electrical Engineering
Stony Brook University
Stony Brook, USA
fang.luo@stonybrook.edu

Kiruba S. Haran
Electrical Engineering
University of Illinois
Urbana Champaign, USA
kharan@illinois.edu

***Abstract*— Cable connected motor winding insulation is prone to failures owing to standing wave overvoltages (OV), caused by switching transition dV/dt. Standing wave is impacted by the motor drive system differential mode and common mode impedance interactions, as well as excitation frequency dV/dt. Winding and cable impedance create a complex combination of resonances and antiresonances. Wide band gap power electronics generate high dV/dt that exacerbates the OV phenomenon. According to the literature, the overvoltage across the motor winding is not distributed evenly between the turns. First turns are reported to be under higher overvoltage where OV is lower and more similar for the subsequent turns. However, in this paper with the accurate HF modeling of the motor drive system, the overvoltage distribution across the turn-to-turn (TT) of the motor winding for different dV/dt is investigated. It is proved that the voltage distribution trend does not remain constant. First, it is due to the different resonances across different TT in an unsymmetric network of drive system. Second, according to the trapezoidal waveform, different dV/dt excitation introduces different bandwidth of the secondary harmonics contributed to the OVs. So, not always the first turn is under highest voltage. Not clear understanding of the OVs could cause insulation overdesign for the first turns or easier degradation of the lateral turns. In this regard, this paper gives a guideline to study the system in regards of impedance interactions with excitation dV/dt in the WBG applications. Therefore, based on this study the appropriate insulation or filtering design to alleviate the OVs can be decided. The ground truth experimental validation for high frequency modeling of the system under test is provided.**

Keywords—DM and CM impedances, turn-to-turn overvoltage distribution, motor winding, reliability, PWM based drive system, Wide Band Gap devices.

I. Introduction

Emerging application of wide band gap (WBG) devices in motor drives systems brings higher dV/dt to the system while the new generation design of high power density motor drive with low winding impedance are growing. The combination of these factors brings higher challenges in insulation design [1]. Despite its advantages, advent of WBG devices lead to new concern in the reliability of the system. High dv/dt leads to high frequency signatures causing EMI, partial discharge concerns. The transient voltages caused by traveling waves through the cable between the inverter and the motor can cause higher motor side overvoltages (OV) referred as reflected wave phenomenon (RWP) [1], causing insulation reliability issues as partial discharge. The OVs impacted by differential mode (DM) impedance interactions and Dv/dt, so OVs and EMI DM signature are coupled. Due to the mix mode discussed in [2], the Common mode noise also varies. So, the study of the OVs in this paper gives an understanding on the basis of the possible variations in EMI signature as well. However, characterization of this high frequency phenomena is complex owing to increased dV/dt and distributed nature of motor drives through DM and CM parasitic elements, see Fig. 1.

Turn-to-turn (TT) insulation failures are reported as the most frequent insulation difficulties in the drive-fed induction motors [3]. Even though much work has been done in RWP characterization and quantification, still the gap with emerging applications of WBG devices and high-power density motors remains, including accurate understanding of the distribution of the OVs across TT of the motor winding.

WBG devices have shorter voltage rise times with higher spectral frequency components, raising the risk of severe peak voltages developed between winding turns during transients [4]. As a result of that, there is a more uneven voltage distribution in the stator winding. The OVs need to be acknowledged otherwise the earlier degradation/failure of the insulation of the system can happen because of HF phenomenon like partial discharge (PD) [5].

Several research has been conducted on uneven voltage distribution across motor winding. A nonuniform voltage distribution among the motor winding coil in different positions of the coil as well as TT is determined by combined different values of R, L and C values of them. Each RLC network acts as a filter, so as going towards the lateral turns beginning from the first turn powered, the OV reported to be decreases [6]. So, in the literature [6-8], always the first turn is reported to be under highest OV.

Furthermore, a couple of studies are done to investigate the impact of dV/dt on the OVs [3,4] and [8,9]. It is reported that the higher dV/dt, cause higher OV amplitude across the TTs.

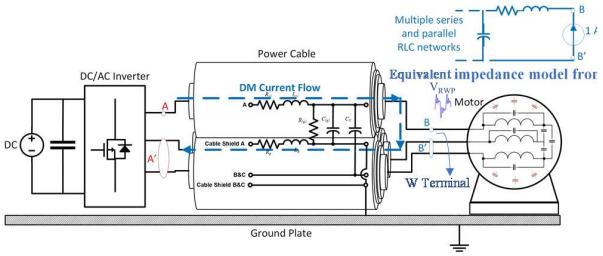

Fig. 1. Cable connected motor drive system schematic

In [9], a different distribution of OV is reported because of different capacitive networks of a quasi-random wound-motor compared to random wound one. This does not give a general guideline on the motor drive system's different configurations, and it specifies it for quasi-random-wound motor windings. It also points out that by increased dV/dt the OV across TT increases, linearly. However, it is shown in this paper that by variation of dV/dt the trend of the OV distribution across different TT changes and does not remain in same ratios.

In [3,4] and [8,9], it is shown that the dV/dt changes the amplitude of the OVs but not the trend of distribution among different turns. Also, the dV/dt increase/decrease is directly related to increase/decrease in OVs. However, the accurate study of the resonance networks and OV harmonics given in this paper opposes this.

The design network is subject to system layout variation. Hence, modification with varying cable lengths and grounding infrastructures introduces different type of resonance networks across the local junctions, which in this paper is the different TT of the motor winding. So, it is paramount to understand degradation as well as system sensitivity to such layout variation. Therefore, it is necessary to reconsider this local OVs and include this knowledge in system layout, insulation, and filter design.

To address the mentioned research gaps, in this paper, the motivation is to accurately investigate the OV distribution across TT of the motor winding through DM impedance measurement. Besides, the guideline is provided to give a solid analysis of OV harmonics to predict the voltage distribution across TT of the motor winding under excitation dV/dt, which is not limited to a specific kind of system configuration/layout or cable and motor type. In this regard:

- By accurate study of the resonance networks of the power drive system across the local junctions' (here TT) OV harmonics, the general belief on highest OV on first turns of the motor winding could be reconciled.
- It is shown that the trend of the transient voltage distribution across motor winding TT differs varying dV/dt.

Following the guideline throughout the paper:

- Avoids the overdesign of the insulation for first TT as general considerations.
- The appropriate insulation design among the TT of the motor windings and filtering solution for the application under excited dV/dt could be concluded.

The next sections of the paper are as follows.

First, the system under test and the impedance parameters involved in this study is introduced and modeled. It should be noticed that the modeling is inspired by our group published works and is only provided to show the possibility of the prediction of the OV across TT in design level or before testing by accurate modeling of such a system. Then, the modeling is validated. After that, the voltage distribution across TT of the motor winding is investigated varying excitation dV/dt. The approach to predict the OVs is discussed by having both accurate modeling of the system and knowledge on the OV harmonics bandwidth.

II. Motor Drive System Modeling and Impedance Characterization

Cable and motor winding in WBG motor drives heavily attributes to high-frequency noise, owing to impedance mismatch OVs, high frequency mutual coupling, skin effect [10] and eddy currents [11]. These parasitic elements are layout and length dependent. So, the requirement of modeling is to be adaptable with system configuration and extensible for HF. In the following subsections the modeling process in this paper for such a motor drive system is given. The modeling details are published in our group works and referred to in this paper. So, the accurate modeling will provide the possibility to combine it with the information on OV resonance harmonics and excitation dV/dt effect in the next section to predict the OVs.

A.HF Cable Modeling

Length extendibility and infrastructural robustness of cable modeling can be achieved by rigorous cable impedance characterization and RWP experiments using double pulse test (DPT). In this paper, 1 m cable is used to connect the converter with motor windings. In this study, coils are used as the sample of motor winding in a DPT drive system to represent the guideline on OV distribution across TT of the motor winding throughout the paper. The detailed methodology of the cable modeling is shown in Appendix A [11,12], which explains a sequential and hybrid simulation-experiments approach [11,12]. It uses R-L and R-C ladders to represent skin and proximity effect respectively as suggested in Fig. 2(a). The parasitic extraction can be divided into self, CM and DM impedance measurements. The extraction equations are as suggested in [11] and outlined in Appendix B. The self-experiments are used for extraction of cable inductance and resistance as L_{s1}, R_{s1} and mutual coupling. The CM experiments can further be decomposed into open circuit configuration which results in C_{lg1}, C_{lg2}, R_{lg1} and R_{lg2}, proximity effect parameters. The skin inductance and resistance defined as L_{s2}, R_{s2} lead to increased resistance at HF extracted using DM experiments suggested in [11].

B.HF Coil Modeling

The HF model for a form wound coil under test is an impedance network comprised of nodes connected by inductive, resistive, and capacitive elements [13,14]. Each-

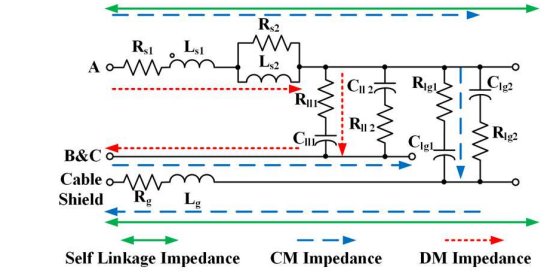

(a)

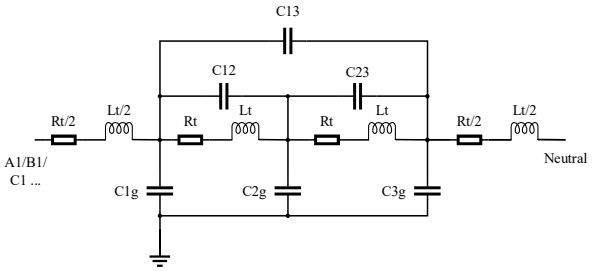

(b)

Fig. 2. High frequency model (a) cable (b) coil

node represents an individual turn in the coil. Fig. 2(b) shows a network model for a 3-turn coil. The network can be extended by adding more nodes and associated elements to incorporate more turns or multiple phases. L_t, R_t, C_{ij} and C_{ig} represent inductance per turn, resistance per turn, capacitance between any two turns and capacitance between turn and ground, respectively. Turn inductance is a lumped parameter includes both self-inductance and turn-turn mutual inductance. Analytical determination of the parameters is given in Appendix C [15,16].

C. HF Converter Modeling

Similar to cable and motor modeling, converter parasitic extraction also plays an important role in accurate modeling of HF phenomena. The parasitic inductance and its distribution along the power loop impacts the dV/dt and OV peak. In this regard, the converter parasitics are extracted using Ansys Q3D. The value of the DPT board parasitics is negligible compared to the cable and motor winding impedance parameters in such a case study. So, their impact on the OVs resonance frequency and magnitude can be neglected in this paper. Otherwise, it is recommended to consider the converter parasitics in the modeling as well.

III. Impedance Model Validation

A standardized test bench is setup complying with DO-160G standard [16] to validate the modeling of the system including converter, cable and coil. The cables and coils for impedance measurements are set up using Bode 100 Network Analyzer in the same test bed as for DPT shown in Fig. 3. Further, the CM and DM impedance for cable and coil from simulation and actual hardware measurement are plotted in Fig. 4. The simulation and actual measurements are in agreement with each other.

The test conducted for various voltage levels, using CREE half bridge CRD8FF650P DPT board. For the measurements, the load terminal voltage and coil TT voltages were measured with Tektronix THDP0200 200 MHz differential probes.

Similarly, two 1 GHz oscilloscopes MSO56 by Tektronix were utilized to have precise and accurate measurements. Fig. 5 shows the load terminal voltage waveforms using 1 m cable superimposed in frequency and amplitude in simulation and practical DPT. This can assure of the accurate modeling, so the OV distribution across TT of the motor winding, could

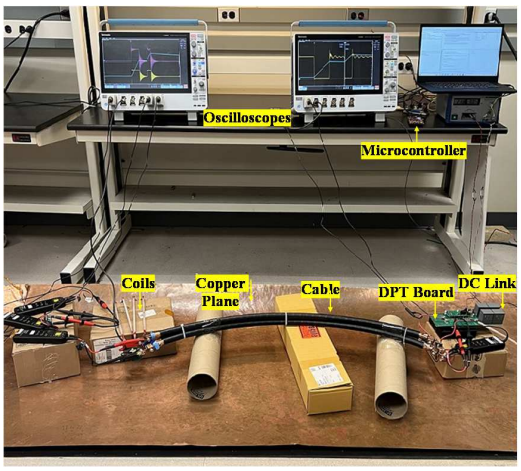

Fig. 3. RFW DPT setup

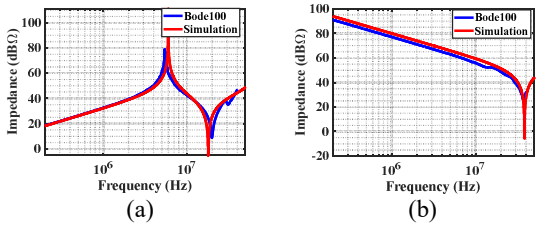

Fig. 4. Cable and coil impedance. (a) DM (b) CM

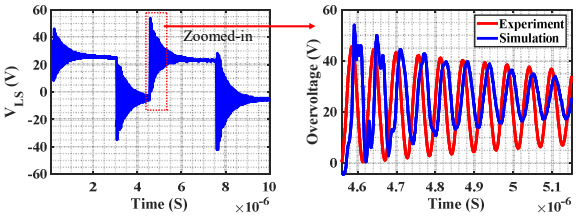

Fig. 5. RFW results matching in practical and simulation DPT at load terminal using 1 m cable

be predicted using this model and knowledge on the OV resonance harmonics' bandwidth.

IV. Voltage Distribution on Motor Winding Turn-Turn

An analytical framework is needed for WBG power electronics motor drives that can be used to determine insulation design guidelines for PD-free operation. So, by considering the HF drive system modeling and the dV/dt excitation of the WBG devices, the different trend in OV distribution across the TT of the motor winding could be seen and investigated and predicted by the approach given in the following.

A. DV/dt Impact on Turn-Turn Voltage Distribution

In practical DPT test, the volatge across TT of the coil is measured by removing a small part of the insulation on turns of the coils and demonstarted as waveforms of the volatge across first turn to second turn ($V_{TT\text{-}12}$) and second turn to third turn ($v_{TT\text{-}23}$) in Fig. 6. The DPT results for the TT voltages is shown for input source voltage of 100 and 500 V subsequently switching converter with low and high dV/dt, respectively shown in Fig. 6 (a) and (b). Also, the results in Fig. 6 (c) is shown for the 500V input source voltage but the motor winding coils are placed in a different hight to the copper plane. To compare the OVs across turns, as it can be seen from the zoomed-in area from the DPT results, the peak of the $v_{TT\text{-}12}$ is higher than $v_{TT\text{-}23}$ for low dV/dt excitation and is lower for high dV/dt, respectively in Fig. 6 (a) and (b). However, the voltage distribution remains almost the same for TT-12 and TT-23 for the test case conducted under same conditions as the second scenario with the same dV/dt but with different coil placement. This shows the importance of the drive systme impedance interactions as well as dV/dt of excitation source variation to design the free PD system or provide appropriate solutions like insulation or filtering design to avoid early degradation.

B. Discussion on the Trend of OV Distribution Across TT

The FFT of TT voltages in Fig. 6, is shown in Fig. 7 (a) and (b), respectively for low and high dV/dt. The difference in the amplitude of the OVs harmonic across different TT and

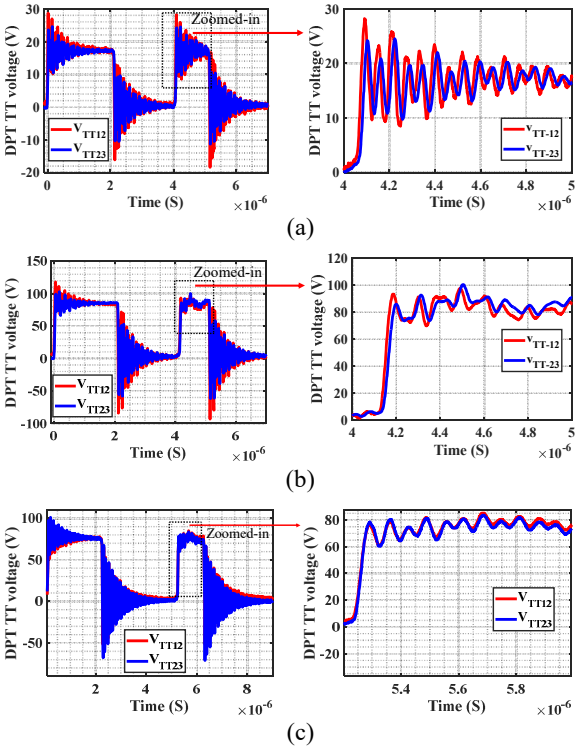

Fig. 6. Experimental results for turn-turn voltage distribution (a) low dV/dt (b) high dV/dt (c) high dV/dt but different configuration of the coils

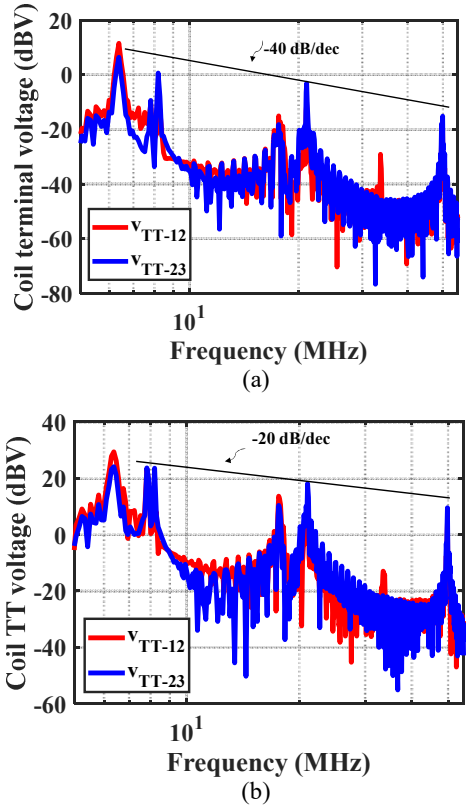

Fig. 7. Harmonics trend in TT overvoltages (a) low (b) high dV/dt

also different trends of the voltage distribution among TTs with different excitation dV/dt could be explained as follows.

1- The OV resonance harmonics are different in amplitude and phase across different TT. This is due to the different resonance network in DM impedance (unsymmetric network), across each of the TT winding, caused by geometry and location of the motor winding turn. Hence, the vector sum of the OV harmonics comes up with different amplitude of the OV for TT_23 and TT_23.

2- A square/trapezoidal shape voltage/current source shown in Fig. 8 is modeled as switching devices, as the main noise sources in power electronic devices [18].

More intuitive information from the harmonic spectra and investigation of the effect of rising/falling time and pulse width is effectively extracted from the spectral bounds of the waveform FFT.

Fig. 8. shows the harmonic spectrum of a trapezoidal waveform. So, the harmonic spectrum in Fig. 8 (b) starts with 0 dB/decade up to the first breakpoint $f1=1=\pi\tau$. The value drops with the slope of -20 dB/decade up to $f2=1/\pi\tau r$. Beyond this point, the magnitude drops by the slope of -40 dB/decade. Fig. 8 describes how fast the short rise and fall times increase the bandwidth of the noise sources.

So, as shown in Fig. 8 (a) and (b), trapezoidal harmonic bounds in low dV/dt and high dV/dt differ. And higher dV/dt, the lower risetime in this study, excitation increases the bandwidth of harmonics. The segment with -20 dB/dec slope will make more contribution in the total OV. However, as shown in Fig. 8 (a), with lower dV/dt, higher risetime, the secondary harmonics decrease with the slope of -40 dB/dec.

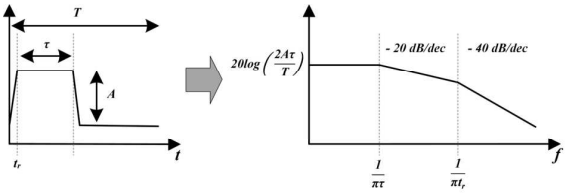

Fig. 8. Harmonic spectrum of a trapezoidal waveform

Thus, the secondary harmonics contribute less to the total OV. As different TT has different magnitude of harmonics shown in Fig. 7. Therefore, the OV peak ratios differ for different TT with varying the excitation dV/dt. Hence, it should be noted that the voltage distribution could be different due to the unsymmetric TT harmonics and the dV/dt. Not always the higher dV/dt will cause the linear increase in the OVs, but it is TT harmonics' ratio to each other and their bandwidth under the excitation. This implies that accurate modeling of the system, knowledge on OV harmonics across each TT and knowledge of dV/dt contribution in OV harmonics bandwidth aids in estimating OV distribution in motor winding.

Further, two tests in paper [4] with the same test setup is conducted to investigate the impact of RFW voltage amplitude in PD occurrence under 20kHz unipolar square wave excitation. The first PDIV is observed at 750 V. The voltage level increased from 750 V to 800 V increases PD amplitude and number of pulses with PD event. Thus, it is shown increasing the voltage level has noticeable impact on

PD occurrence. Therefore, TT OV with higher peak values can significantly deteriorate and damage the insulation over time which shows the importance of the study in this paper.

V. Conclusion

The impact of the dV/dt value on peak transient TT OV distribution is a striking demonstration of the challenges imposed by modern WBG switches on machine windings. In this paper, the guideline is provided to study and predict the OV distribution across the TTs of a motor winding. It is shown that due to the unsymmetric resonance network of a motor drive system, the OV harmonics across different TT of the winding is not the same. So, due to the magnitude of the harmonics and the bandwidth that excitation dV/dt provides for the harmonics, the voltage distribution trend could vary. This investigation opposes the usual consideration of the highest OV for the first turns. This paper gives a guideline to design the TT insulation and filtering solutions in a motor drive system, accurately. As it is known that in sensitive applications like aircraft, due to the high-altitude conditions like less pressure, PD has lower inception voltages. So, the inaccurate acknowledge on the TT OVs causes serious failure.

The resonance network in an unsymmetric system like the one discussed in this paper is very sensitive to DM and CM impedance parameter changes. So, by the strategical study given in this paper for any other motor drive system, the TT OV distribution could be predicted. This could save costs by not overdesigning the insulation which could also lead to high power density system design. Furthermore, shows the importance of the taking care of the secondary harmonics in filter design in the case of higher dV/dt not just in case of reliability of the first TTs but also the subsequent TTs.

Acknowledgment

This project was supported by the U.S. Federal Aviation Administration under Grant 692M15-20-C-00010." Also, the authors would like to acknowledge the National Science Foundation (NSF Award No. 1846917) for lending financial support for this work.

References

[1] B. Narayanasamy and et. al., "Reflected wave phenomenon in SiC motor drives: consequences, boundaries, and mitigation," *IEEE transactions on power electronics,* vol. 35, no. 10, pp. 10629-10642, 2020.

[2] W. Zhou, X. Pei, Y. Xiang and Y. Kang, "A new EMI modeling method for mixed-mode noise analysis in three-phase inverter system," *IEEE Access,* vol. 8, pp. 71535-71547, 2020.

[3] F. Endrejat, and P. Pillay, "Resonance overvoltages in medium-voltage multilevel drive systems," *IEEE Transactions on Industry Applications,* vol. 45, no. 4, pp. 1199-1209, 2009.

[4] T. H. Zhu, and H. Borcherding, "Investigations on the Influences of Winding Positions and Rise Times on the Winding Isolation System within the Line-End Coil under Fast Rising Impulse Voltages," *IEEE EPE'21 ECCE Europe*, 2021.

[5] S. Salehi Vala, K. Choksi, A. B. Mirza, F. Luo, "Exploring Interactions Between Reflected Wave and Partial Discharge in WBG Motor Drives," *IEEE ECCE*, 2022.

[6] M. Pastura, S. Nuzzo, G. Franceschini, G. Sala, & D. Barater, "Sensitivity analysis on the voltage distribution within windings of electrical machines fed by wide band gap converters," IEEE *ICEM,* vol. 1, 2020.

[7] H. Ting, and H. Borcherding, "Investigations on the Influences of Winding Positions and Rise Times on the Winding Isolation System within the Line-End Coil under Fast Rising Impulse Voltages," *IEEE EPE'21 ECCE Europe,* 2021.

[8] F. Rodrigo, and A. C. Ferreira, "Influence of the Surge Rise-Time on the Turn-to-Turn Transient Voltage Distribution in Rotating Machine Stator Windings using a Three-Phase Model," *EIC*, 2021.

[9] H. Zeng, J. Swanke, T. M. Jahns &B. Sarioglu, "High-frequency modeling and inter-turn voltage distribution analysis of a modular electric machine for electric aircraft propulsion," *IEEE ITEC*, 2022.

[10] N. Idir, Y. Weens, and J. J. Franchaud, "Skin effect and dielectric loss models of power cables," *IEEE Transactions on Dielectrics and Electrical Insulation*, vol. 16, no. 1, pp. 147-154, 2009.

[11] Y. Wu, K. Choksi, M. ul Hassan and F. Luo, "An Extendable and Accurate High- Frequency Modelling of Three-phase Cable for Prediction of Reflected Wave Phenomenon," *IEEE index APEC*, 2022, pp. 944-950.

[12] K. Choksi, Y. Wu, and F. Luo. "Evaluation of Factors Impacting Reflected Wave Phenomenon in WBG Based Motor Drives," *IEEE index IPEC-Himeji-ECCE Asia*, 2022.

[13] O. A. Mohammed and et.al., "High frequency PM synchronous motor model determined by FE analysis," *IEEE transactions on magnetics*, vol. 42, no. 4, pp. 1291-1294, 2006.

[14] P. Brauer, "High-frequency voltage distribution modelling of a slotless PMSM from a machine design perspective," *M.S. thesis, EEC Dept., KTH Univ.,* Stockholm, Sweden, 2018.

[15] X. Zhang, K. S. Haran, and J. Xiao, "Analytical Calculation of Equivalent Circuit Parameters and Operational Inductance in Multiple-Pole Slotless PMSMs," *IEEE ITEC*, 2022.

[16] T. Jokinen, V. Hrabovcova, and J. Pyrhonen, "Design of rotating electrical machines," John Wiley & Sons, 2013.

[17] I. RTCA, "Environmental conditions and test procedures for airborne equipment," *Radio Technical Commission for Aeronautics*, Washington, DC, USA, Tech. Rep., 2007.

[18] F. Abolqasemi Kharanaq, A. Emadi, and B. Bilgin, "Modeling of conducted emissions for EMI analysis of power converters: State-of-the-art review," *IEEE Access,* vol. 8, pp. 189313-189325, 2020.

Appendix

A.

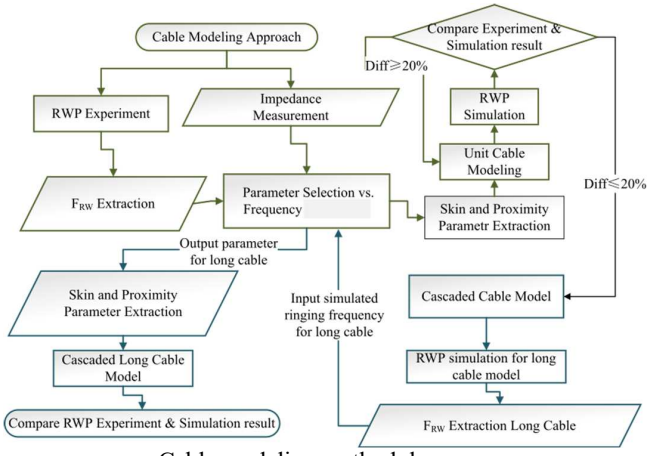

Cable modeling methodology

B.

HF cable modeling parasitic elements extraction

$$R_{DM,SF} = 2R_{s1} \quad (1)$$

$$L_{DM,SF} = 2(L_{s1} - M_{ll}) \quad (2)$$

$$L_{DM,SF} = L_{s1} \quad (3)$$

$$R_{s2} = \frac{R_{DM,HF} - R_{DM,LF}}{2} \quad (4)$$

$$L_{s2} = \frac{L_{DM,LF} - L_{DM,HF}}{2} \quad (5)$$

$$C_{lg1} = \frac{L_{CM,SF}}{3} \quad (6)$$

$$C_{lg2} = \frac{L_{CM,LF}}{3} \quad (7)$$

$$R_{lg2} = \frac{R_{CM,HF} - R_{CM,LF}}{2} \quad (8)$$

$$R_{DM,SF} = R_{lg1} \quad (9)$$

$$C_{CM,SF} = \frac{2}{3}C_{lg1} + 2C_{ll} \quad (10)$$

$$R_g = R_{SF} \quad (11)$$

$$L_g = L_{SF} \quad (12)$$

$$L_{CM,SF} = L_g + L_{s1} - 2M_{lg} \quad (13)$$

C.

The figure below shows a machine slot structure with a 3-turn coil sitting inside it. The width, height, and axial length of one turn are W_t, H_t, and l_t, respectively. This geometry will be used as an example to determine the parameters in Fig. 2(b).

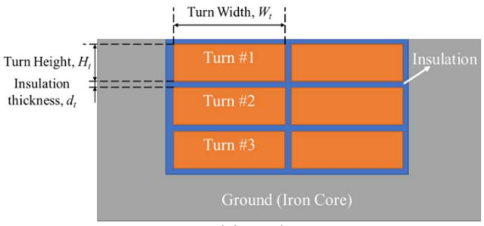

Machine slot structure

Turn DC resistance is determined by Ohm's Law, i.e.,

$$R_{DC} = \frac{l_t}{\sigma_c k_{fil} W_t H_t} \quad (14)$$

where σ_c is the copper conductivity and k_{fil} is the copper fill factor. However, the turn resistance also increases with the excitation frequency due to skin and proximity effects. A resistance factor is introduced:

$$R_t = k_R R_{DC} \quad (15)$$

At very high frequencies, k_R is approximately [15,16]

$$k_R \approx \frac{2z_t^2+1}{3}\xi \quad (16)$$

where z_t is the number of turns, and ξ is the reduced conductor height, defined as

$$\xi \approx H_t\sqrt{\frac{1}{2}\omega\mu_0\sigma_c\frac{2W_t}{W_s}} \quad (17)$$

where ω is the electrical frequency, μ_0 is void permeability, W_s is the slot width.

Turn inductance consists of two parts, i.e., self-inductance and turn-turn mutual inductance. They need to be found by solving the magnetic circuit either analytically or through finite element (FE) modeling methods. For the test setup where no iron core is used, the inductance obtained from a magnetostatic FE model. For the slotted structure, a simple magnetic circuit analysis gives the self-inductance as

$$L_t = \frac{\mu_0\tau_p l_t}{k_c g} + L_\sigma \quad (18)$$

where τ_p is pole pitch (circumferential distance between both sides of one coil), g is the airgap length, k_c is Carter's coefficient, and L_σ is the leakage inductance. Turn-turn mutual inductance within one phase is given as

$$M_t = \frac{\mu_0\tau_p l_t}{k_c g} \quad (19)$$

Capacitance between two conductors is determined by their distance and the dielectric constant of the insulation material. For example, the parasitic capacitance between Turn #1 and Turn #2 can be calculated as

$$C_{12} = \frac{\varepsilon_r\varepsilon_0 W_t l_t}{d_t} \quad (20)$$

where ε_r and $d_t$are the dielectric constant and thickness of the insulation material, ε_0 is the vacuum permittivity. The expressions for other capacitive elements can be derived in a similar way [15,16].